arXiv:1610.00038v1 [cond-mat.str-el] 30 Sep 2016

Non-collinear Order and Spin-Orbit Coupling in Sr_3ZnIrO_6

P. A. McClarty *,[1] A. D. Hillier,[1] D. T. Adroja †,[1,2] D. D. Khalyavin,[1]
S. Rayaprol,[3] P. Manuel,[1] W. Kockelmann,[1] and E. V. Sampathkumaran[4]

[1]*ISIS Neutron and Muon Source, Rutherford-Appleton Laboratory, Harwell Campus, Oxfordshire, OX11 0QX, UK*
[2]*Highly Correlated Electron Group, Physics Department, University of Johannesburg, P.O. Box 524, Auckland Park 2006, South Africa*
[3]*UGC-DAE CSR, Mumbai Center, R-5 Shed, BARC, Trombay, Mumbai 400085, India*
[4]*Tata Institute of Fundamental Research, Homi Bhabha Road, Colaba, Mumbai 400005, India*

(Dated: October 4, 2016)

Sr_3ZnIrO_6 is an effective spin one-half Mott insulating iridate belonging to a family of magnets which includes a number of quasi-one dimensional systems as well as materials exhibiting three dimensional order. Here we present the results of an extensive investigation into the magnetism including heat capacity, a.c. susceptibility, muon spin rotation (μSR), neutron diffraction and inelastic neutron scattering on the same sample. It is established that the material exhibits a transition at about 17 K into a three-dimensional antiferromagnetic structure with propagation vector $\boldsymbol{k} = (0, \frac{1}{2}, 1)$ in the hexagonal setting of R$\bar{3}$c and non-collinear moments of $0.87\mu_B$ on Ir^{4+} ions. Further we have observed a well defined powder averaged spin wave spectrum with zone boundary energy of ~ 5 meV at 5 K. We stress that a theoretical analysis shows that the observed non-collinear magnetic structure arises from anisotropic inter- and intra- chain exchange which has its origin in significant spin-orbit coupling. The model can satisfactorily explain the observed spin wave excitations.

PACS numbers: 75.30.Cr, 75.30.Ds, 75.30.Gw, 75.4, 75.25.-j, 0.Gb, 75.40.Mg, 75.47.Lx

In materials with Ir^{4+} ($5d^5$, $S = 1/2$) ions occurring in IrO_6 octahedral units, spin-orbit entanglement combined with the crystal field lead to an effective description in terms of interacting spin one-half moments. Exploring such magnetic systems has been a topic of intense study over the last few years motivated by the search for novel electronic phases including topological insulators, complex magnetic structures, quantum spin liquids and other exotica. For example, in various 2D and 3D honeycomb lattice magnets, strong spin-orbit coupling leads to Ising exchange along bonds joining magnetic ions which may lead to Kitaev spin liquids being realized in solid state magnets[1–3]. The iridate pyrochlores have provided a rich set of interesting phenomena and inspired new ideas to realize novel phases[4]. More recently, the electron doped layered iridate Sr_2IrO_4 has been shown to have tantalizing similarities to the hole-doped precursors of the high temperature superconductors[5].

In this paper, we consider iridate magnetism in yet another context: in Sr_3ZnIrO_6 - one of a family of magnetic materials with chemical formula $A_3BB'O_6$ in which magnetic ions live on the B or B' positions or both and where A is either Sr^{2+} or Ca^{2+}. Recent interest in this family of materials among condensed matter physicists stems from the fact that when both B and B' are magnetic the materials often exhibit quasi-1D Ising magnetism and that the magnetic chains have a triangular coordination giving the potential for geometrical frustration to affect their ground states[6–9]. The most well-known case is $Ca_3Co_2O_6$[6,7,10–13] which has ferromagnetically coupled chains with weak antiferromagnetic inter-chain correlations. However, many of these materials are phenomenologically interesting: there is evidence for partially disordered antiferromagnetism at low temperatures in $Ca_3Co_2O_6$[10–13], Ca_3CoRhO_6[14] and Sr_3NiIrO_6[8,15] co-existing with peculiar dynamical properties including memory effects. In sharp contrast, Ca_3NiMnO_6[16] exhibits spiral order at low temperatures while Ca_3CoMnO_6 exhibits collinear-magnetism-driven ferroelectricity[17]. In all these materials, the inter-chain coupling plays a crucial role. In order to appreciate better the nature of these couplings, one may substitute nonmagnetic ions onto the B site so that the inter and intra chain couplings become comparable which is the case in Sr_3ZnIrO_6[18].

Early work on Sr_3ZnIrO_6 reported the crystal structure determined from X-ray measurements and both the moment size and the scale of the exchange coupling from the d.c. susceptibility but no 3D long-range magnetic ordering transition was observed in the neutron diffraction work[18,19]. Subsequent studies based on a.c. and d.c. magnetization as well as heat capacity (C_p) measurements established the existence of long-range magnetic ordering in this material[20]. In this paper, we present results of an extensive experimental investigation into the magnetic properties of this material including a.c. susceptibility, heat capacity, muon spin rotation (μSR), neutron diffraction and inelastic neutron scattering culminating in the determination of the magnetic structure in this material and its excitations. The magnetism of Sr_3ZnIrO_6 is *a priori* expected to be affected significantly by spin-orbit coupling. We present a theoretical model that explains the non-collinear spin structure in this material based on exchange parameters which rely on the presence of significant spin-orbit coupling. Our theory establishes the most general form of the couplings that can arise between magnetic B site ions.

Experimental Methods - The compound Sr_3ZnIrO_6 was prepared by the solid-state route as detailed in Ref. 20. The quality of the sample was checked using x-ray and neutron diffraction measurements and found to be a single phase.

*paul.mcclarty@stfc.ac.uk
†devashibhai.adroja@stfc.ac.uk

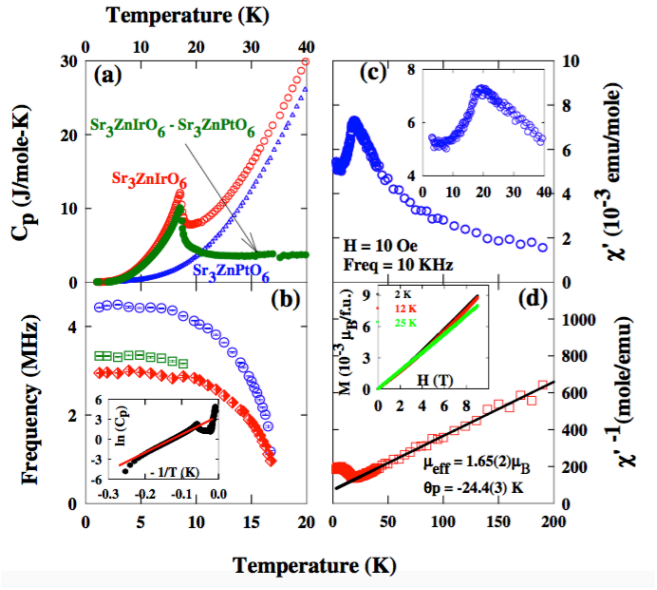

FIG. 1: **(Color online) Experimental characterisation of the magnetism in Sr_3ZnIrO_6.** (a) Heat capacity of Sr_3ZnIrO_6 and the magnetic part obtained by subtracting that of Sr_3ZnPtO_6 (also shown). (b) Triplet of μSR frequencies vs. temperature showing onset at T_N. Inset: exponential fit to magnetic heat capacity. (c) a.c. susceptibility χ' vs. temperature with inset showing vicinity of T_N. (d) Curie law in paramagnetic regime with magnetization isotherms at various temperatures plotted in the inset..

The ac-magnetization and heat capacity, C_p, measurements were carried out using a Quantum Design physical properties measurement system (PPMS). The neutron diffraction measurements were carried out on the GEM and WISH time-of-flight diffractometers at the ISIS facility. The powder sample of Sr_3ZnIrO_6 contained in a vanadium can of 3-mm diameter was placed inside a standard helium cryostat under He-exchange gas on WISH. The temperature dependent order parameter was measured on the GEM diffractometer. The μSR experiment was performed on the MuSR spectrometer at the ISIS facility.

Experimental Results - Here we discuss our experimental results on Sr_3ZnIrO_6. Fig. 1 shows the temperature dependent heat capacity, a.c. magnetic susceptibility and μSR frequency. As we can see in Fig. 1a in zero field a clear lambda type anomaly is observed near 17 K in $C_p(T)$, which is indicative of a transition to long-range magnetic order. The room temperature value of the heat capacity is 225 J/mole-K, which is close to 274 J/mole-K, the value expected for the lattice contribution with 11 atoms per unit cell[21]. To estimate the phonon contribution we have also plotted the Sr_3ZnPtO_6 heat capacity data in Fig. 1a between 2.4 K and 50 K. When the total measured heat capacity data were plotted as C_p/T vs. T^2 for Sr_3ZnIrO_6 the data below 12 K exhibited linear behavior, $C_p = \gamma T + AT^3$, which gave $\gamma \approx 4.5$ mJ/mole-K^2 and $A = 1.438$ mJ/mole-K^4. A contains both spin-wave and lattice contributions so it is not possible to determine a reliable value of the Debye temperature for Sr_3ZnIrO_6. A similar method applied to the nonmagnetic reference compound, Sr_3ZnPtO_6 gave a Debye temperature of $396(4)$ K. In order to estimate the magnetic contribution of the heat capacity, we subtracted the lattice contribution using the Sr_3ZnPtO_6 data. The magnetic contribution is plotted in Fig. 1a. We have observed an entropy of 2.39 J/mole-K at 20 K compared to 5.17 J/mole-K expected for S=1/2. We have estimated the spin gap by plotting $\log(C_{\rm mag})$ vs $1/T$ which gave a value of 13.8 K (1.2 meV) (see inset Fig. 1b).

The ac susceptibility was measured between 2 and 300 K in a magnetic fields of 10 Oe over a range of frequencies. The real part of the ac susceptibility χ' shows a peak at 17 K due to an antiferromagnetic ordering of the Ir moments Fig. 1c which is independent of frequency between 10 Hz and 10^4 Hz[22]. For temperatures greater than 25 K the inverse susceptibility vs. temperature plot follows the expected Curie Weiss (CW) behavior Fig. 1d, which gives an effective magnetic moment, $1.65(2)\mu_B$ and a CW temperature, $-24.4(3)$ K. The value of the observed magnetic moment is close to the 1.73 μ_B expected for $S = 1/2$ in agreement with previous studies[19,20].

The temperature dependence of the muon spin relaxation was measured in a zero field. For all temperatures above $T_N = 17$ K, the muon spin relaxation spectra can be described by a simple exponential decay. However, on cooling below 17 K, coherent oscillations are observed in the μSR spectra (see Fig. S4 in the supplementary section). This shows that we have a long-range magnetically ordered ground state. The μSR spectra are well described by three sinusoidal functions with a Gaussian envelope and an exponential decay. The temperature dependence of the three observed μSR frequencies are plotted in Fig. 1c. Below 8 K we have three well resolved frequencies, but above 8 K two lower frequencies merge together. The overall temperature dependence of the observed frequencies is consistent with that expected for a second order phase transition.

Figure 2 shows a neutron diffraction pattern collected at 1.5 K from the WISH diffractometer. At this temperature, there are four weak additional Bragg peaks (marked with stars) compared to the pattern collected in the paramagnetic state at 25K (not shown here). The fact that these observed magnetic peaks disappear above 17 K (see inset Fig. 2), indicates that the magnetic ordering temperature is 17 K in agreement with μSR and heat capacity. The intensities of the superstructure peaks decrease with momentum transfer (Q) confirming their magnetic origin. The peak positions can all be indexed by the propagation vector $\boldsymbol{k} = (0, 1/2, 1)$ in the hexagonal setting of the R$\bar{3}$c space group. This is a high-symmetry point of the Brillouin zone, labeled k_5 in the Kovalev notation and equivalent to $\boldsymbol{k} = (1/2, 1/2, 0)$ in the rhombohedral setting. The symmetry analysis shows that there are four one-dimensional representations in the little group, labelled τ_i $(i = 1, 4)$ in Kovalev notation,[23] but only two enter in the decomposition of $\Gamma = 3\tau_1 + 3\tau_3$. Both IR have three basis vectors, $\phi_{1,i}$ and $\phi_{3,i}$ $(i = 1, 2, 3)$. We first tried to fit the magnetic structure using τ_3, but we were unable to fit the intensities and positions of all observed magnetic reflections. Considering now τ_1, we found that none of the $\phi_{1,i}$ modes taken separately give a satisfactory agreement with the data. However,

a solution is found by refining a model with a linear combination of the three modes. The final refinement yields a good description of the experimental data (Fig. 2) and a magnetic Bragg factor RB = 14%, as obtained by a fit with the software FULLPROF[24]. The mixing coefficients for the three modes $\phi_{1,i}$, $i = 1, 2, 3$ are respectively -0.072, -0.579 and 0.670 and the ordered state Ir moment of $0.87(3)$ μ_B. It is to be noted that the moment has three components -0.072, -0.579 and 0.670 along the a,b and c-axis respectively. The magnetic structure of Sr_3ZnIrO_6 is same as that of Sr_3ZnRhO_6[25]. Thus the magnetic structure is non-collinear, with a substantial angular deviation of the magnetic moment with respect to the c axis. Consequently, the threefold symmetry axis is lost, and the magnetic transition corresponds to a change of magnetic point group from 3m.1' in the paramagnetic state to 2/m.1' in the magnetically ordered state. The observation of three frequencies in the muon data is also consistent with the loss of threefold symmetry. A representation of the magnetic structure is displayed in Fig. 2c.

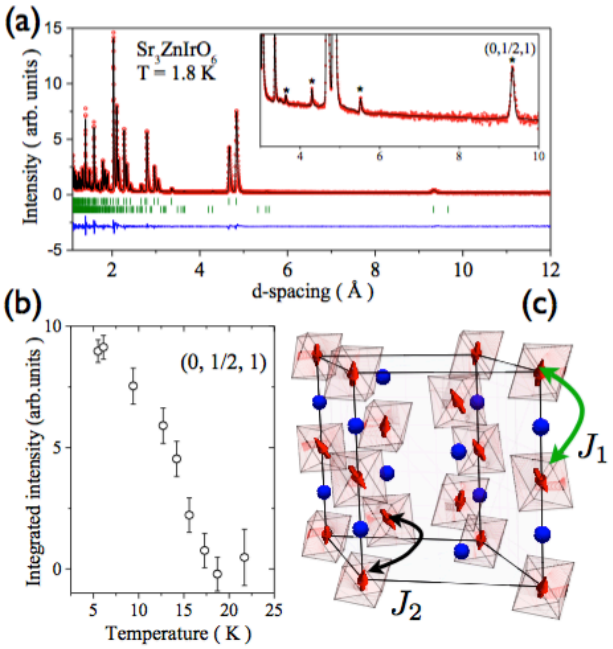

FIG. 2: **(Color online) Experimental characterisation of the magnetism in Sr_3ZnIrO_6.** (a) Neutron diffraction pattern at 1.8K of Sr_3ZnIrO_6 from the bank-2 at 58.2 degrees of WISH . The symbols show the experimental data and the line shows the fit using nuclear and magnetic structures. The blue line at the bottom shows the difference plot and vertical bars indicate the Bragg peak positions: nuclear at the top and magnetic at the bottom. The inset shows the data on an expanded scale where stars show the observed magnetic Bragg peaks. (b) The temperature dependent intensity of magnetic (0, 1/2, 1) peak measured on GEM. (c) The crystal structure in the hexagonal setting with Ir (red), Sr (blue) and the oxygen octahedra. The magnetic structure in the cell is also shown together with the nearest neighbor and next nearest neighbor bonds.

Exchange Couplings – The existence of three dimensional magnetic order without a regime of purely 1D correlations

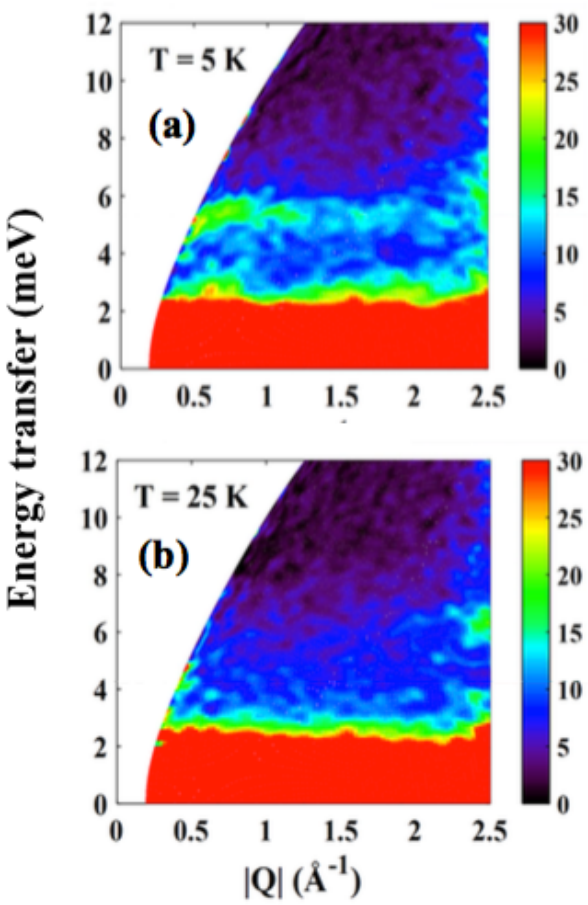

FIG. 3: **(Color online) Color coded inelastic neutron scattering intensity maps.** Energy transfer vs. momentum transfer measured with an incident energy of $E_i = 18$ meV on MERLIN for two different temperatures - one above and one below T_c.

above T_c indicates that the scale of the further neighbor exchange is similar to that of the intra-chain exchange in Sr_3ZnIrO_6. In an iridate one expects, *a priori*, the spin-orbit coupling to be relevant to the low temperature magnetic order[26]. This expectation is confirmed by the discrete nature of the symmetry breaking into a state with moments in the ab plane that are orientated almost along the bond directions. In order to understand the origin of the magnetic structure of Sr_3ZnIrO_6, isotropic exchange is therefore not sufficient so we determine the most general bilinear couplings allowed by the lattice symmetries and then establish the minimal set of couplings that are necessary to select the observed magnetic structure.

For nearest neighbors within the chains along the c axis, there are three possible types of exchange: Ising, isotropic easy plane and Dzyaloshinskii-Moriya[27]. The latter coupling has $\boldsymbol{D}$ vectors along the c direction and alternating in sign from one bond to the next. The second neighbor interactions couple iridium ions in different chains. The chains are arranged in a triangular lattice but with three different staggerings in the c direction such that the second neighbor coordi-

nation is in the form of a puckered hexagon. One may show that there are six distinct types of second neighbor exchange coupling. Of these six, one couples the Ising components and three couple the XY components, one of which preserves the global $U(1)$ symmetry. The remaining two couple XY to Z components and are central to selecting the observed structure in Sr_3ZnIrO_6. Further details on the symmetry analysis and explicit forms for the second exchange can be found in the Supplementary Material.

Classical Phases − Having established the nature of the exchange couplings in Sr_3ZnIrO_6 and related materials with significant spin-orbit coupling, we may find the possible magnetically ordered phases. We obtain the ground states of the exchange model by rotating the vector spins along their local mean field on a periodic cluster. As guidance for this calculation - in particular, to choose the correct minimal cell for the minimization - we obtain the ordering wavevector $\mathbf{Q}_{\rm ord}$ from the location $\mathbf{q} = \mathbf{Q}_{\rm ord}$ of the minimum eigenvalue of the Fourier transformed interactions $\mathcal{J}_{ab}(\mathbf{q})$ where a and b are the 6 magnetic sublattices in the hexagonal representation of the interactions.

Exchange to nearest neighbor only couples moments within chains running along the c axis. Further neighbor couplings are necessary for fully three dimensional ordered structures. For example, the second neighbor XY antiferromagnetic coupling leads to spontaneous symmetry breaking to a collinear XY structure identical to the one observed in Ca_3ZnMnO_6[28]. A collinear structure with moments along the c axis is found for second neighbour Ising exchange.

One obtains the structure close to that observed in Sr_3ZnIrO_6 and Sr_3ZnRhO_6 by including couplings for exchanges $H_{z\pm,\rm as}$ (antisymmetric) and $H_{z\pm,\rm s}$ (symmetric) in the ratio $J^{(2)}_{z\pm,\rm s}/J^{(2)}_{z\pm,\rm as} = \sqrt{3}$ with both couplings negative. Then one may switch on either antiferromagnetic nearest neighbor Ising exchange $J^{(1)}_{\rm zz}$ or second neighbor ferromagnetic Ising exchange $J^{(2)}_{zz}$. The phase diagram obtained with fixed $J^{(2)}_{z\pm,\rm s}/J^{(2)}_{z\pm,\rm as}$ and variable $J^{(1)}_{\rm zz}$ and $J^{(2)}_{zz}$ is shown in Fig. S1 in the supplementary section. There are two distinct ground states. The one for large $|J^{(2)}_{\rm zz}|$ is a simple collinear ferromagnet with $\mathbf{Q}_{\rm ord} = 0$ and the other is proximate to the Sr_3ZnIrO_6 and Sr_3ZnRhO_6[25] antiferromagnetic structure with $\mathbf{Q}_{\rm ord} = (0, 1/2, 1)$. The moments are canted away from the c axis by an angle which is represented by the colored contours in Fig. S1. The experimental value of about 39 degrees is indicated by a black dashed line.

The Sr_3ZnIrO_6 and Sr_3ZnRhO_6 structures differ from the $(0, 1/2, 1)$ phase shown in Fig. S1 by a staggered rotation $\delta\phi_i$ of the moments in the ab plane away from the $60n$ degree angles where the magnitude of $\delta\phi_i$ is the same for all sites. The relevant rotation angle is about 6 degrees for Sr_3ZnIrO_6. Just such a rotation can be achieved by switching on an antiferromagnet XY coupling between nearest neighbor moments.

Magnetic Excitations − The color-coded INS intensity maps of Sr_3ZnIrO_6 measured at 5 K and 25 K with $E_i = 18$ meV are shown in Fig. 3. At $T = 5$ K, with the momentum transfer $|Q|$ below 1.5 Å^{-1}, a strong inelastic scattering peak which shows weak dispersion can be clearly observed between 3 and 6 meV. The magnetic origin of the strong scattering in the $3-6$ meV band is established by the initial reduction in the energy-integrated inelastic intensity as a function of $|Q|$. Further, at 25 K there is no sign of scattering between $3 - 6$ meV. We attribute the observed magnetic excitations between 3 and 6 meV for $|Q|$ below 2 Å^{-1} to spin wave scattering from Ir^{4+} ions in the magnetically ordered state below 17 K , as expected. The spin wave excitations do not survive above $T_N = 17$ K, which is consistent with the proposed similarity between inter and intra chain interactions. In contrast, the spin wave excitations in Sr_3NiIrO_6 survive up to 250 K, which is well above $T_N = 70$ K in that material, indicating the existence of a one-dimensional magnetic exchange interaction[29].

On the basis of the exchange model presented above, we compute the spin wave excitations to leading order in a Holstein-Primakoff $1/S$ expansion. The spectrum has 12 modes albeit with some degeneracies. The spectrum is gapped as we should expect on the basis of the observed discrete symmetry breaking. We are able to obtain the absolute scale of the exchange parameters on the basis of a comparison between the experimental data and the calculated scattering. The powder averaged dynamical structure factor for a set of parameters that give the correct magnetic structure as their semiclassical ground state is shown in Fig. S3 in the supplementary section. A form factor for Ir^{4+} has been applied using parameters from Ref. 30. The model captures the principal features of the INS data including the single strong band of intensity between 4 meV and 6 meV which is clearly visible in both plots and a minimum between 0.5 and 1Å^{-1}. While our exchange parameters are consistent with the available data there is some freedom to choose these parameters while holding the magnetic structure fixed. Single crystal inelastic neutron scattering may be used to determine these parameters completely.

To summarize, we have studied the magnetism in Sr_3ZnIrO_6 using a variety of techniques including heat capacity, ac susceptibility, μSR, neutron diffraction and inelastic neutron scattering. These reveal a clear magnetic transition at 17 K into a fully 3D long range ordered magnetic structure with propagation vector $(0, 1/2, 1)$ in which the moments in the ordered phase exhibit a discrete coplanar orientation with respect to the principal lattice directions. We have also presented a theoretical analysis with which we have understood the origin of the observed magnetic structure. By determining the complete set of allowed couplings between first and second neighbors we establish the importance of anisotropic inter-chain exchange between the XY component of one moment and the Ising component of its neighbor. The model presented here is applicable to both the simple structure observed in Ca_3ZnMnO_6 and the complex non-collinear ordering reported here which is also present in Sr_3ZnRhO_6[25] and Sr_3MgIrO_6[31].

P.M. acknowledges an STFC Keeley-Rutherford fellowship. D.T.A. and A.D.H. acknowledge financial assistance from CMPC-STFC grant number CMPC-09108.

[1] G. Jackeli and G. Khaliullin, Phys. Rev. Lett. **102**, 017205 (2009).
[2] J. Chaloupka, G. Jackeli, G. Khaliullin, Phys. Rev. Lett. **105**, 027204 (2010).
[3] S. K. Choi *et al.*, Phys. Rev. Lett. **108**, 127204 (2012).
[4] W. Witczak-Krempa, G. Chen, Y.-B. Kim, and L. Balents, Annu. Rev. Condens. Matter Phys. **5** 57 (2014).
[5] B. J. Kim, H. Jin, S. J. Moon, J.-Y. Kim, B.-G. Park, C. S. Leem, J. Yu, T.W. Noh, C. Kim, S.-J. Oh, J.-H. Park, V. Durairaj, G. Cao, and E. Rotenberg, Phys. Rev. Lett. **101**, 076402 (2008); Y. K. Kim, N. H. Sung, J. D. Denlinger and B. J. Kim, Nat. Phys. **12**, 37 (2016); Y. K. Kim, et al. Science **345**, 187 (2014).
[6] See, for instance, S. Rayaprol, K. Sengupta, and E.V. Sampathkumaran, Solid State Commun. **128**, 79 (2003); E.V. Sampathkumaran, N. Fujiwara, S. Rayaprol, P.K. Madhu, and Y. Uwatoko, Phys. Rev. B **70**, 014437 (2004); S. Agrestini, L. C. Chapon, A. Daoud-Aladine, J. Schefer, A. Gukasov, C. Mazzoli, M. R. Lees, and O. A. Petrenko, Phys. Rev. Lett. **101**, 097207 (2008).
[7] See, for instance, T. Basu, K.K. Iyer, K. Singh, and E.V. Sampathkumaran, Sci. Rep. **3**, 3104 (2013); A. Jain, P. Y. Portnichenko, H. Jang, G. Jackeli, G. Friemel, A. Ivanov, A. Piovano, S. M. Yusuf, B. Keimer, and D. S. Inosov, Phys. Rev. B **88**, 224403 (2013).
[8] E. Lefrancois, L. C. Chapon,V. Simonet, P. Lejay, D. Khalyavin, S. Rayaprol, E.V. Sampathkumaran, R. Ballou, and D. T.Adroja, Phys. Rev. B **90**, 014408 (2014).
[9] X. Ou and H. Wu, Sci. Rep. 4, 4609 (2014).
[10] H. Kageyama *et al.*, J. Phys. Soc. Jpn **66** 1607 (1997).
[11] A. Maignan et al., J. Mater. Chem. **14**, 1231 (2004).
[12] V. Hardy et al., Phys. Rev. B **70**, 064424 (2004); ibid. **70**, 214439 (2004).
[13] C. L. Fleck, M. R. Lees, S. Agrestini, G. J. McIntyre and O. A. Petrenko, EPL **90**, 67006 (2010).
[14] S. Niitaka *et al.*, Phys. Rev. Lett. **87** 177202 (2001).
[15] D. Mikhailova,B. Schwarz,A. Senyshyn, A. M. T. Bell,Y. Skourski,H. Ehrenberg,A. A. Tsirlin, S. Agrestini, M. Rotter, P. Reichel,J. M. Chen, Z. Hu, Z. M. Li,Z. F. Li, and L. H. Tjeng, Phys. Rev. B **86**, 134409 (2012).
[16] S. Kawasaki *et al.*, J. Solid State Chem., **145** 302 (1999); S. Rayaprol, Kausik Sengupta, E.V. Sampathkumaran, and Y. Matsushita, J. Solid State Chem. **177**, 3270 (2004);
[17] Y. J. Choi, H. T. Yi, S. Lee, Q. Huang, V. Kiryukhin, and S.-W. Cheong, Phys. Rev. Lett. **100**, 047601 (2008).
[18] T.N. Nguyen and H.-C. zur Loye, J. Solid. Chem. **117**, 300 (1995).
[19] Christina Lampe-Önnerud, Manfred Sigrist, and Hans-Conrad zur Loye, J. Solid State Chem., **127** 25 (1996).
[20] Asad Niazi, E.V. Sampathkumaran, P.L. Paulose, D. Eckert, A. Handstein, and K.-H. Mueller, Solid State Commun. **120**, 11 (2001); Asad Niazi, E.V. Sampathkumaran, P.L. Paulose, D. Eckert, A. Handstein, and K.-H. Mueller, Phys. Rev. B **65**, 064118 (2002).
[21] N. W. Ashcroft and N. D. Mermin, Solid State Physics (W. B. Saunders Company, Philadelphia, PA), p. 427. (1976).
[22] Supplementary Section.
[23] O. V. Kovalev (ed.), *Representation of the Crystallographic Space Groups* (Gordon and Breach, Newark, NJ, 1993).
[24] J. Rodriguez-Carvajal, FULLPROF 2k, Version 2.0c, July 2002, Lab. Leon Brillouin, 2002.
[25] A. D. Hillier *et al.*, Phys. Rev. B. **83**, 024414 (2011).
[26] Y. Yamaji, Y. Nomura, M. Kurita, R. Arita, and M. Imada Phys. Rev. Lett. **113**, 107201, (2014).
[27] I.Dzyaloshinskii, Journal of Physics and Chemistry of Solids **4**, 241 (1958); T. Moriya, Physical Review **120**, 91 (1960).
[28] M Y Ruan, Z W Ouyang, Y M Guo, J J Cheng, Y C Sun, Z C Xia, G H Rao, S Okubo and H Ohta, J. Phys.: Condens. Matter **26** 236001 (2014).
[29] S. Toth, W. Wu, D. T. Adroja, S. Rayaprol, and E. V. Sampathkumaran, Phys. Rev. B **93**, 174422 (2016).
[30] K. Kobayashi, T. Nagao and M. Ito, Acta Cryst., **67** 473 (2011).
[31] D. T. Adroja, C. Ritter. L. Pascut, A.D. Hillier, *et al.*, unpublished

Supplementary Section

I. SYMMETRIES

The starting point for our analysis is the set of crystal symmetries. Here we refer to the hexagonal setting of the $R\bar{3}c$ space group. The point group symmetry at the magnetic sites (Wyckoff sites $6b$) is S_6 which, apart from the trivial element, is composed of 3-fold rotations about the c axis, inversion and S_6 operations which are 6-fold rotations about the c axis followed by reflection through the ab plane passing through the origin. There are two other symmetry operations. The first is a reflection about one of the three planes containing a magnetic ion and two of its (hexagonally coordinated) second neighbours followed by a translation in the c direction by $(0, 0, 1/2)$. The second is a rotation about one the three axes in the ab plane passing through the magnetic ion and the midpoints of two of its second neighbours followed by a translation along the c axis through $(0, 0, 1/2)$.

There are two magnetically inequivalent sites. We label sites i, a using the convenient body centered rhombohedral setting where $a = 1, 2$ is the sublattice and i is the rhombohedral cell. The nearest neighbor couplings connect the two different sublattices. With this exchange alone, the magnetic structure splits up into decoupled chains. Each site has six second nearest neighbors which also connect different sublattices.

II. EXCHANGE COUPLINGS BETWEEN B IONS

We first consider the number of exchange parameters allowed between nearest neighbours. The 2 nearest neighbours of each magnetic ion are in the c direction and their coupling alone results in a lattice of decoupled chains. In this case we can write

down the allowed couplings with little analysis. There are three such couplings: one is the Ising coupling $\sum_{i,a,b} S^z_{i,a} S^z_{i,b}$ where i runs along the chains, the second is the isotropic XY coupling $(1/2)\sum_{i,a,b} S^+_{i,a} S^-_{i,b} + S^-_{i,a} S^+_{i,b}$. The third is the Dzyaloshinskii-Moriya interaction $\sum_{i,a,b} \mathbf{D}_{a\to b} \cdot (\mathbf{S}_{i,a} \times \mathbf{S}_{i,b})$ with $\mathbf{D}_{a\to b}$ vector along the c axis and alternating in sign between adjacent bonds.

Now we focus on the couplings between second neighbors. First we can compute the number of second neighbour exchange parameters allowed by the local point group symmetry. Then we impose the remaining constraints coming from the symmetries that involve translations.

The second neighbors form a puckered hexagon around the central magnetic ion (see Fig. 5). Before imposing symmetry constraints, each bond contributes 9 couplings of the form $S^\alpha_i S^\beta_j$ for fixed sites i and j and there are six bonds. All these couplings transform under some representation $\Gamma_{\rm M}$. We find that $\Gamma_{\rm M} = 9A_g \oplus \ldots$ and these 9 couplings are further reduced when we consider symmetries that involve translations.

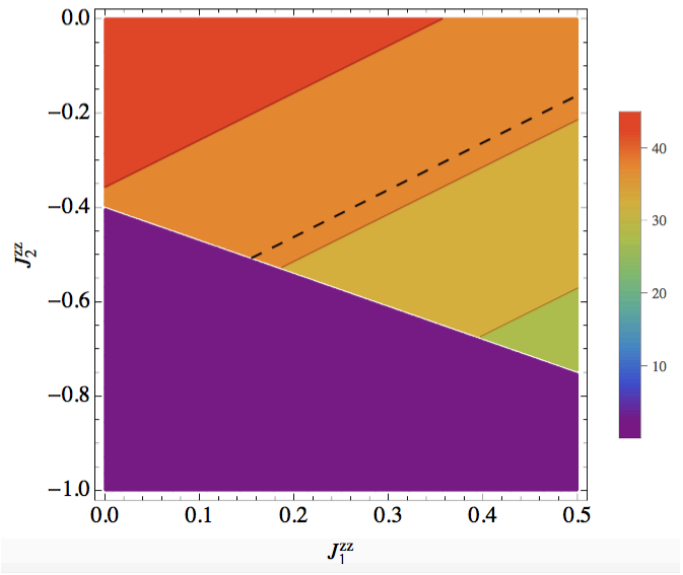

FIG. 4: (Color online) **Phase diagram with two types of Ising exchange and $J^{(2)}_{z\pm,\rm s}$, $J^{(2)}_{z\pm,\rm as}$ fixed.** The diagram shows two phases. At the bottom of the diagram, the blue region is the collinear ferromagnetic phase. The second phase is the magnetic structure of Sr_3ZnIrO_6 up to a small rotation of the moments in the XY plane. The gradient of colors in the latter phase represents the canting angle of the moments with respect to the c axis.

The glide and rotation-translation symmetries reduce the number of linearly independent exchange couplings from 9 to 6. They may be divided into three couplings that have $U(1)$ symmetry which are

$$
\begin{aligned}
H_{\rm zz} =& J^{(2)}_{\rm zz} \sum_{\langle\langle i,aj,b\rangle\rangle} S^z_{i,a} S^z_{j,b} \\
H_{\rm xy} =& \frac{J^{(2)}_{\rm xy}}{2} \sum_{\langle\langle i,aj,b\rangle\rangle} \left(S^+_{i,a} S^-_{j,b} + S^-_{i,a} S^+_{j,b} \right) \\
H_{\rm DM} =& J^{(2)}_{\rm DM} \sum_{\langle\langle i,aj,b\rangle\rangle} \boldsymbol{D}_{a\to b} \cdot (\boldsymbol{S}_{i,a} \times \boldsymbol{S}_{j,b}) \,,
\end{aligned}
$$

where $\boldsymbol{D}_{a\to b} = \pm\hat{\boldsymbol{z}}_c$ along the one-dimensional chains with $+$ for $a = 1$ and $b = 2$ and minus otherwise. Then there are three exchange operators that are invariant only under discrete symmetries. These are most conveniently represented by considering

six particular sites shown in Fig. 5 where j_1 is separated from i in the $\hat{\boldsymbol{y}}$ direction:

$$H_{++} = \frac{J^{(2)}_{++}}{2} \sum_i \left(S^+_{i,1} S^+_{j_1,2} + e^{-2\pi i/3} S^+_{i,1} S^+_{j_2,2} + e^{2\pi i/3} S^+_{i,1} S^+_{j_3,2} + S^+_{i,1} S^+_{j_4,2} + e^{-2\pi i/3} S^+_{i,1} S^+_{j_5,2} + e^{2\pi i/3} S^+_{i,6} S^+_{j_6,2} \right) + \text{h.c.}$$

$$H_{z\pm,\text{as}} = \frac{J^{(2)}_{z\pm,\text{as}}}{2} \sum_i \left(S^+_{i,1} S^z_{j_1,2} - S^z_{i,1} S^+_{j_1,2} + \ldots \right) + \text{h.c.}$$

$$H_{z\pm,\text{s}} = \frac{J^{(2)}_{z\pm,\text{s}}}{2} \sum_i i \left(S^+_{i,1} S^z_{j_1,2} + S^z_{i,1} S^+_{j_2,2} + \ldots \right) + \text{h.c.}$$

While H_{++} is given in full, the ellipses in the expressions for $H_{z\pm,\text{as}}$ and $H_{z\pm,\text{s}}$ indicate those exchange couplings obtained by performing symmetry operations on the one bond joining $i, 1$ and $j_1, 2$.

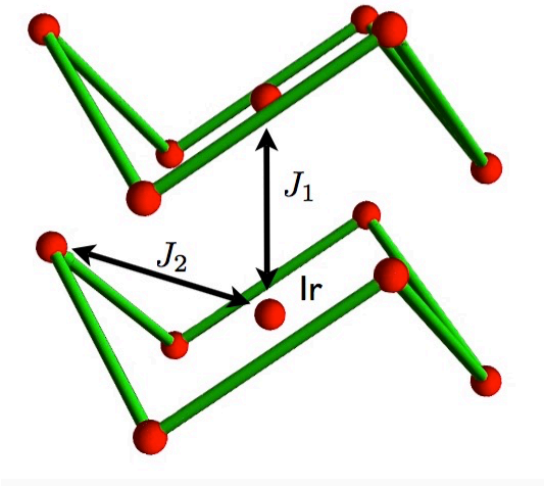

FIG. 5: (Color online) Figure showing the hexagonally coordinated second neighbors about each Ir ion.

The correct magnetic structure for Sr_3ZnIrO_6 is obtained as follows. We set $J^{(2)}_{z\pm,\text{s}} = \sqrt{3} J^{(2)}_{z\pm,\text{as}}$ which selects the required structure up to a small rotation of moments in the XY plane and up to a canting angle from the c axis. This constraint is apparently fine-tuned and we conjecture it is fixed by the microscopic superexchange mechanism. The magnetic structure is stable to the presence of Ising couplings to first and second neighbor as shown in the phase diagram Fig. 4. The structure is also robust to a nonzero $J^{(2)}_{++}$ coupling and we make use of this fact to fit the spin wave intensity. In order capture the exact structure we also switch on a small second neighbor $J^{(2)}_{\text{xy}}$ coupling. The couplings are given explicitly in the caption to Fig. 6

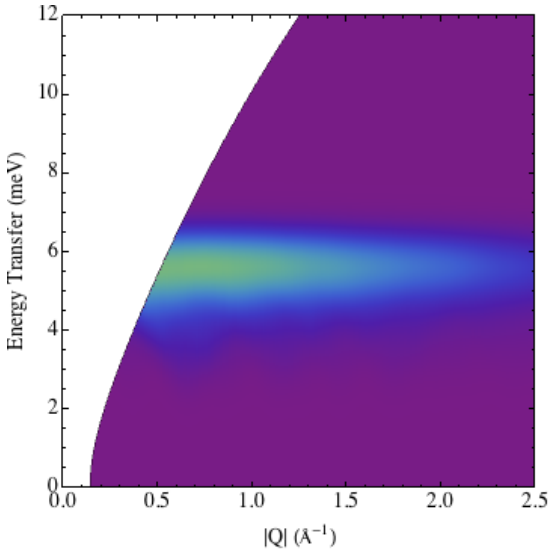

FIG. 6: **(Color online) Angular averaged spin wave intensity computed to linear order in** $1/S$ The exchange parameters are only weakly constrained by the observed magnetic structure. For the spin wave calculation we chose the following couplings (in meV) $J^{(1)}_{\rm zz} = 0.3$, $J^{(1)}_{\rm xy} = 0.135$ to first neighbor and $J^{(2)}_{\rm zz} = -0.525$, $J^{(2)}_{\pm} = 0.263$, $J^{(2)}_{z\pm,\rm as} = -0.18$ and $J^{(2)}_{z\pm,\rm s} = -0.311$ to second neighbor.

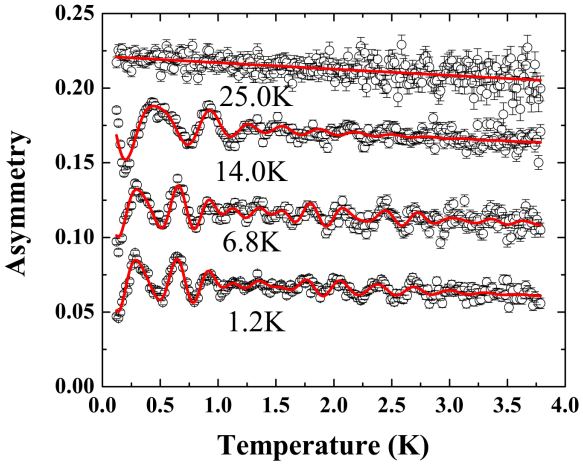

FIG. 7: (Color online) muSR asymmetry measured at four different temperatures. Oscillations are clearly visible at 14 K and below. Analysis of this data leads to the three distinct frequencies plotted in Fig. 1 (b) of the main paper.